Weakening of tensile strength of granitic rock by HV-HF-AC actuation of piezoelectric properties of Quartz: a 3D numerical study

T Saksala[1], R A Rubio Ruiz[2], A Kane[3] and M Hokka[2]

[1]Faculty of Built Environment, [2]Faculty of Engineering and Natural Sciences, Tampere University, Finland
[3]Sintef Industry, Norway

timo.saksala@tuni.fi

Abstract. High-voltage and high-frequency alternating current (HV-HF-AC) excitation of piezoelectric properties of Quartz is a potential method to induce cracks in granite. This was recently shown in a numerical feasibility study [6], where cracking was induced on cylindrical rock samples made of granite by sinusoidal AC excitation at the frequency of ~100 kHz and the amplitude of ~10 kV. However, this study did not investigate the weakening effect due to this cracking on the tensile strength of the sample. The present study addresses this topic numerically. For this end, a numerical method based on 3D embedded discontinuity finite elements for rock fracture and an explicit time stepping scheme to solve the coupled piezoelectro-mechanical problem is adopted. Rock heterogeneity and anisotropy are accounted for at the mineral mesotructure level. A preliminary numerical simulation demonstrates that the HV-HF-AC treatment reduces the tensile strength of a cylindrical granite sample by 12 %, making it thus a potential non-conventional pre-treatment method in comminution and excavation of Quartz bearing rocks and ores.

1. Introduction

Low energy efficiency and excessive tool wear are the major problems in comminution and excavation of rocks and ores [1, 2]. For this reason, new energy efficient methods are presently being intensively searched. In particular, the unconventional techniques, i.e. nonmechanical or noncontact techniques, especially those exploiting electricity, used either alone or as a rock weakening pre-treatment prior to mechanical comminution have drawn extensive attention lately [3, 4, 5].

One such method uses high-voltage and high-frequency alternating current (HV-HF-AC) excitation of piezoelectric properties of Quartz in granite to induce cracking by the converse piezoelectric effect. Saksala [6] carried out a numerical feasibility study on this new method and showed that it has some promise. Namely, damage in the form of cracks was inflicted on cylindrical rock samples made of granite by sinusoidal AC excitation at the frequency of ~100 kHz and the amplitude of ~10 kV. In order to induce cracks, the frequency of the excitation needed to match one of the natural frequencies of the sample. The fracture mechanism was thus related to the resonance phenomenon appearing in forced vibration of the sample. It was also shown in this study that inducing cracks by converse piezoelectric effect using direct current is impossible, as the voltage required exceeds the electric breakdown strength (100–150 kV/cm for granite) of the rock. In this case, the sample would thus fracture due to the plasma channel spallation effect.

However, the study by Saksala [6] did not investigate the weakening effect due to the cracking induced by piezoelectric excitation on the tensile strength of the sample. Therefore, the present study addresses this important topic by a numerical study. More specifically, a cylindrical specimen is first treated by piezoelectric excitation and then subjected to uniaxial tension test. For this end, the numerical method based on 3D embedded discontinuity finite elements for rock fracture and the explicit time stepping scheme to solve the coupled piezoelectro-mechanical problem developed in ref. [6] is employed. This method accounts for rock heterogeneity and anisotropy at the mineral mesotructure level. Numerical simulations are carried out to demonstrate the weakening effect.

2. Theory of the modelling approach

2.1. Discontinuity plane in a finite element discretized piezoelectric material

Consider a 3D body made of piezoelectric material discretized with 4-node tetrahedral elements under electric field **E**. Assume the body also to be split into two (or more) disjoint parts by a displacement discontinuity, i.e. a crack, as illustrated in Figure 1. Displacement discontinuity Γ_{di} $(i=1,2)$ is defined by the normal $\mathbf{n}_d$ and tangent vectors $\mathbf{m}_1$, $\mathbf{m}_2$.

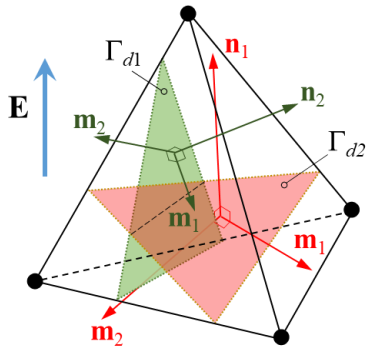

Figure 1. 4-node tetrahedron with two intersecting discontinuity planes

With the small deformation assumption (valid for rock at room temperature and low confinement pressure), the displacement and strain fields for such element are

$$\begin{aligned}\mathbf{u} &= N_i\mathbf{u}_i^e + \sum_{k=1}^{2} M_{\Gamma_{dk}}^e \boldsymbol{\alpha}_{dk}, \quad \text{with} \quad M_{\Gamma_{dk}}^e = H_{\Gamma_{dk}} - \varphi_{\Gamma_{dk}} \\ \boldsymbol{\varepsilon} &= (\nabla N_i \otimes \mathbf{u}_i^e)^{sym} - \mathbf{d}\cdot\underbrace{\nabla N_i \phi_i^e}_{\mathbf{E}} - \sum_{k=1}^{2}((\nabla\varphi_{\Gamma_{dk}} \otimes \boldsymbol{\alpha}_{dk})^{sym} + \delta_{\Gamma_{dk}}(\mathbf{n}_{dk} \otimes \boldsymbol{\alpha}_{dk})^{sym})\end{aligned} \tag{1}$$

where the symbols meaning are: $\boldsymbol{\alpha}_{dk}$ is the displacement jump; N_i and $\mathbf{u}_i^e$ are the standard interpolation functions for the linear tetrahedron and nodal displacements (i = 1,..,4 with summation on repeated indices), respectively; **d** is piezoelectric coefficients matrix; ϕ_i^e is the nodal value of the electric potential; $H_{\Gamma_{dk}}$ and $\delta_{\Gamma_{dk}}$ denote the Heaviside function and its gradient, the Dirac delta function; $M_{\Gamma_{dk}}^e$ is a function, which, through function $\varphi_{\Gamma_{dk}}$, restricts the effect of $\boldsymbol{\alpha}_{dk}$ inside the corresponding finite element (for more details see [6]). It should be noted that as the displacement jump is assumed elementwise constant, so that the expression for strain in (1) follows taking the gradient and adding the piezoelectric strain. Moreover, the term containing the Dirac's delta function, in (1), is non-zero only at the discontinuity plane. As this term is zero at the element nodes, it can be neglected at the global level when solving the discretized equations of motion.

2.2. Traction-separation model for solving the crack opening vector

In the present approach, the rock material is taken as linear elastic, but heterogeneous and anisotropic, up to fracture, which is modelled by the embedded discontinuity technology. A fixed (nonrotating) discontinuity (crack) is introduced to an element upon violation of the first principal stress criterion with the discontinuity normal conforming to the first principal direction. Moreover, the Cauchy relation, $\mathbf{t}_{\Gamma_d} = \boldsymbol{\sigma}\cdot\mathbf{n}_d$, between the stress $\boldsymbol{\sigma}$ and traction $\mathbf{t}_{\Gamma_d}$ over the discontinuity plane holds in this approach. The softening process is controlled by a traction-separation law. The present formulation imitates plasticity theory as the crack opening (displacement jump) is irreversible. Furthermore, a loading function is needed for judging between elastic and inelastic stress states. The model components for each crack are (written without the subindex k indicating crack number):

$$\begin{aligned}
&\varphi_d(\mathbf{t}_{\Gamma_d},\kappa,\dot{\kappa}) = \mathbf{n}_d\cdot\mathbf{t}_{\Gamma_d} + \beta\left((\mathbf{m}_1\cdot\mathbf{t}_{\Gamma_d})^2 + (\mathbf{m}_2\cdot\mathbf{t}_{\Gamma_d})^2\right)^{1/2} - (\sigma_{\mathrm{t}} + q(\kappa,\dot{\kappa}))\\
&q = h\kappa + s\dot{\kappa}, \quad h = -g\sigma_{\mathrm{t}}\exp(-g\kappa), \quad g = \sigma_{\mathrm{t}}/G_{\mathrm{Ic}}\\
&\dot{\mathbf{t}}_{\Gamma_d} = -\mathbf{C}_{\mathrm{e}} : (\nabla\varphi_{\Gamma_d}\otimes\dot{\boldsymbol{\alpha}}_d)^{sym}\cdot\mathbf{n}_d, \quad \dot{\boldsymbol{\alpha}}_d = \dot{\lambda}\frac{\partial\varphi_d}{\partial\mathbf{t}_{\Gamma_d}}, \quad \dot{\kappa} = -\dot{\lambda}\frac{\partial\varphi_d}{\partial q}\\
&\dot{\lambda}\geq 0, \quad \varphi_d\leq 0, \quad \dot{\lambda}\varphi_d = 0
\end{aligned} \tag{2}$$

where the symbols are as follows: φ_d is the loading function (equivalent to yield function in plasticity); $\kappa,\dot{\kappa}$ are the internal variable and its rate related to the softening law q for the discontinuity; σ_{t} is the tensile strength; s is the viscosity modulus meaning that the model is strain rate dependent; G_{Ic} is the mode I fracture energy; h is the softening modulus; $\dot{\lambda}$ is the crack opening increment; $\mathbf{C}_{\mathrm{e}}$ is the elasticity tensor; β (= 1 in this study) is the shear control parameter. The third row in (2) shows the evolution laws for traction, crack opening and the internal variable. As the fourth row shows the consistency conditions, the model in (2) can be solved by the standard stress integration (return mapping) algorithm.

2.3. Global solution of the piezoeletro-mechanical problem

The finite element form of the piezoelectro-mechanical problem at time t (ignoring the irrelevant terms) is written as [6]:

$$\begin{aligned}
&\mathbf{M}\ddot{\mathbf{u}}_t + \mathbf{C}\dot{\mathbf{u}}_t + \mathbf{f}_t^{\mathrm{int}}(\mathbf{u}_t,\boldsymbol{\phi}_t) = \mathbf{0}\\
&\mathbf{K}_{\phi\mathrm{u}}\mathbf{u}_t + \mathbf{K}_{\phi}\boldsymbol{\phi}_t = \mathbf{0} \quad \text{with}\\
&\mathbf{M} = \mathbf{A}_{e=1}^{N_e}\int_{\Omega_e}\mathbf{N}_{\mathrm{u}}^{e,T}\mathbf{N}_{\mathrm{u}}^{e}\mathrm{d}\Omega, \quad \mathbf{C} = \alpha\mathbf{M}, \quad \mathbf{f}_t^{\mathrm{int}} = \mathbf{A}_{e=1}^{N_e}\int_{\Omega_e}\mathbf{B}_{\mathrm{u}}^{e,T}\boldsymbol{\sigma}(\mathbf{u}_t,\phi_t)\mathrm{d}\Omega\\
&\mathbf{K}_{\phi} = \mathbf{A}_{e=1}^{N_e}\int_{\Omega_e}\mathbf{B}_{\phi}^{e,T}\boldsymbol{\varepsilon}\mathbf{B}_{\phi}^{e}\mathrm{d}\Omega, \quad \mathbf{K}_{\mathrm{u}\phi} = \mathbf{A}_{e=1}^{N_e}\int_{\Omega_e}\mathbf{B}_{\mathrm{u}}^{e,T}\mathbf{e}\mathbf{B}_{\phi}^{e}\mathrm{d}\Omega, \quad \mathbf{K}_{\phi\mathrm{u}} = \mathbf{K}_{\mathrm{u}\phi}{}^{T}
\end{aligned} \tag{3}$$

where the symbol meanings are as follows: $\mathbf{M}$ is the consistent mass matrix (which is lumped by the row sum technique); $\mathbf{C}$ is the material damping matrix and α is a coefficient; $\mathbf{f}_t^{\mathrm{int}}$ is the internal force vector; $\ddot{\mathbf{u}}_t,\dot{\mathbf{u}}_t,\mathbf{u}_t$ are the acceleration, velocity and displacement vectors, respectively; $\boldsymbol{\phi}_t$ is the electric potential vector; $\boldsymbol{\varepsilon} = \varepsilon\mathbf{I}$ is the (diagonal) dielectric constants matrix; $\mathbf{e} = \mathbf{d}\cdot\mathbf{C}_e$ is the piezoelectric coupling matrix; $\mathbf{A}$ is the standard finite element assembly operator; $\mathbf{N}_{\mathrm{u}}^{e}$ and $\mathbf{B}_{\mathrm{u}}^{e}$ are the displacement interpolation matrix and the kinematic matrix (mapping the nodal displacement into element strains); $\mathbf{N}_{\phi}^{e}$ and $\mathbf{B}_{\phi}^{e}$ are the electric potential interpolation matrix and its gradient.

The first Equation in (3) is the balance of linear momentum while the second is the piezoelectro-static balance. It should be noted that there is no forcing or loading terms in these equations as the loading comes from the essential boundary conditions, i.e., either displacement (in tension test) or the electrical potential (in piezoelectric excitation) which are specified at a part of the model boundary. This problem is solved with a staggered explicit time marching scheme [6]. Finally, the constitutive equation is

$$\boldsymbol{\sigma} = \mathbf{C}_e : (\hat{\boldsymbol{\varepsilon}} - \textstyle\sum_{k=1}^{2}(\nabla\varphi_{\Gamma_{dk}}\otimes\boldsymbol{\alpha}_{\mathrm{d}k})^{sym} - \mathbf{d}\cdot\mathbf{E}) \tag{4}$$

where $\hat{\boldsymbol{\varepsilon}} = (\nabla N_i\otimes\mathbf{u}_i^e)^{sym}$ is the standard FE strain, and the second term is the strain due to crack opening $\boldsymbol{\alpha}_d$, while the third term is the strain due to piezoelectric excitation, i.e. the loading term (note that $\mathbf{E} = -\nabla N_i\phi_i^e$). A new discontinuity (the second cracks) is needed to handle the situation where the first crack in an element due to the piezoelectric treatment is oriented so that it cannot open during the consequent uniaxial tension test. Without another crack, such an element would withstand

unrealistically high stresses. In the present approach, another crack is introduced if the present major principal stress exceeds the tensile strength of the element, and the corresponding principal direction deviates from the first crack orientation more than 45 °. The strength of the new crack is a convex combination of the strength of the intact mineral and the strength of the first crack with the convexity constant being the dot product of the new principal direction and the old crack normal.

2.4. Heterogeneous and anisotropic rock material description

The numerical granitic rock, consisting of α-Quartz (33%), Feldspar (59%) and Biotite (8%), is described as heterogeneous, anisotropic linear elastic fracturing material. The crystal systems for these minerals are trigonal (α-Quartz), triclinic (Plagioclase Feldspar) and monoclinic (Biotite) [7-10]. However, Biotite is considered here as pseudo-hexagonal, and the hexagonal values measured by Alexandrov and Ryzhov [7] are used. The corresponding elasticity matrices and the piezoelectric constants matrix for Quartz are [10]:

$$\mathbf{C}_e^q = \begin{pmatrix} C_{11} & C_{12} & C_{13} & C_{14} & 0 & 0 \\ C_{12} & C_{11} & C_{13} & -C_{14} & 0 & 0 \\ C_{13} & C_{11} & C_{33} & 0 & 0 & 0 \\ C_{14} & -C_{14} & 0 & C_{44} & 0 & 0 \\ 0 & 0 & 0 & 0 & C_{44} & C_{14} \\ 0 & 0 & 0 & 0 & C_{14} & \frac{1}{2}(C_{11}-C_{12}) \end{pmatrix}, \quad \mathbf{d}^q = \begin{pmatrix} d_{11} & -d_{11} & 0 & d_{14} & 0 & 0 \\ 0 & 0 & 0 & 0 & -d_{14} & -2d_{11} \\ 0 & 0 & 0 & 0 & 0 & 0 \end{pmatrix} \tag{5}$$

$$\mathbf{C}_e^f = \begin{pmatrix} C_{11} & C_{12} & C_{13} & C_{14} & C_{15} & C_{16} \\ C_{12} & C_{22} & C_{23} & C_{24} & C_{25} & C_{26} \\ C_{13} & C_{23} & C_{33} & C_{34} & C_{35} & C_{36} \\ C_{14} & C_{24} & C_{34} & C_{44} & C_{45} & C_{46} \\ C_{15} & C_{25} & C_{35} & C_{45} & C_{55} & C_{56} \\ C_{16} & C_{26} & C_{36} & C_{46} & C_{56} & C_{66} \end{pmatrix}, \quad \mathbf{C}_e^b = \begin{pmatrix} C_{11} & C_{12} & C_{13} & 0 & 0 & 0 \\ C_{12} & C_{11} & C_{13} & 0 & 0 & 0 \\ C_{13} & C_{11} & C_{33} & 0 & 0 & 0 \\ 0 & 0 & 0 & C_{44} & 0 & 0 \\ 0 & 0 & 0 & 0 & C_{55} & 0 \\ 0 & 0 & 0 & 0 & 0 & \frac{1}{2}(C_{11}-C_{12}) \end{pmatrix} \tag{6}$$

The rock heterogeneity is described by random clusters of finite elements (see Figure 2c) in the mesh so that each mineral is allotted the percentage of elements in the mesh corresponding to the percentage of each mineral in the rock.

3. Numerical examples

The numerical simulations of uniaxial tension test on the intact and HV-HF-AC-treated samples are described here. The material properties for the minerals, taken from [7-9], used in the simulations are given in Table 1 and 2.

Table 1. Elasticity [GPa] and piezoelectric constants [pC/N] for rock minerals

Quartz	C_{11}	C_{33}	C_{44}	C_{12}	C_{13}	C_{14}	d_{11}	d_{14}
	87.3	105.8	57.2	6.6	12.0	-17.2	2.27	-0.67
Biotite	C_{11}	C_{33}	C_{44}	C_{12}	C_{13}			
	186.0	54.0	5.8	32.4	11.6			
Feldspar	C_{11}	C_{22}	C_{33}	C_{44}	C_{55}	C_{66}	C_{12}	C_{13}
	104.8	190.1	169.3	23.6	32.5	35.6	50.2	42.2
	C_{23}	C_{15}	C_{25}	C_{35}	C_{46}	C_{14}	C_{16}	C_{26}
	18.6	1.13	-0.99	4.14	-2.6	7.34	-4.3	-4.6
	C_{36}	C_{45}	C_{56}					
	-5.2	-0.14	2.6					

Table 2. Material and model parameters for simulations.

Parameter/mineral	Quartz	Feldspar	Biotite
ρ [kg/m^3]	2650	2630	3050
s_d [MPa·s/m]	0.001	0.001	0.001
σ_t [MPa]	10	8	7
G_{Ic} [J/m^2]	40	40	28
ε [F/m]	4.5ε_0	6.3ε_0	7.75ε_0

ε_0 = 8.854E-12 F/m

In Table 2, ε is the relative dielectric constant while ε_0 is that of the vacuum. Moreover, s_d is the viscosity modulus. The boundary conditions and the finite element mesh are shown in Figure 2.

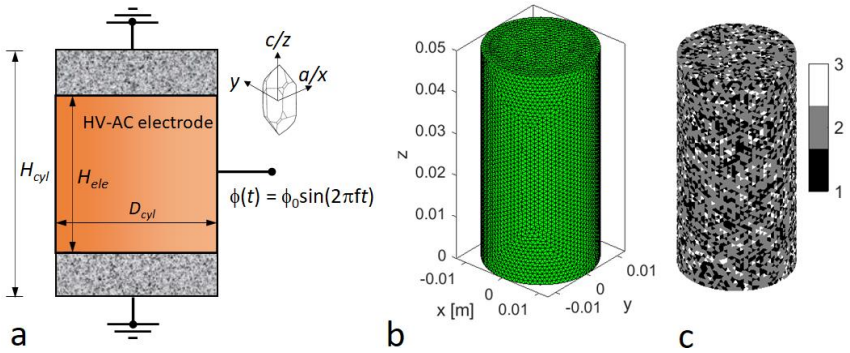

Figure 2. Boundary conditions (H_{cyl} = 50 mm, H_{ele} = 30 mm, D_{cyl} = 25 mm, φ_0 = 50 kV, f = 305 kHz) (a), the finite element mesh with 206617 elements (b), numerical rock mineral texture (3 = Quartz, 2 = Feldspar, 1 = Biotite) (c).

A sinusoidal excitation with 500 cycles was applied on the numerical rock sample, as indicated in Figure 2a. The mineral crystal orientations were assumed, for the sake of demonstration albeit somewhat unrealistically, to align with the global *xyz*-coordinate system so that matrices in (5) and (6) can be readily used (without rotation). Figure 3 shows the results.

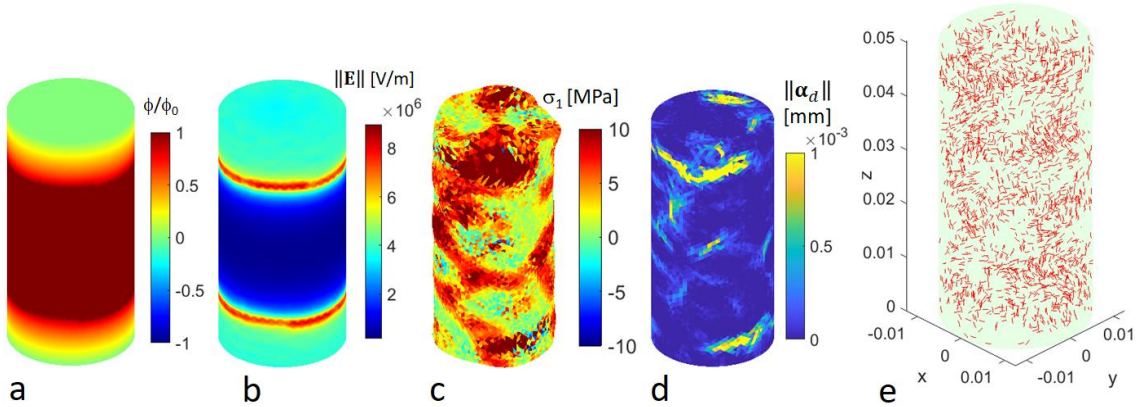

Figure 3. Normalized potential field (a) and the magnitude of electric field at the crest 1st of cycle (b); Major principal stress field (in the 1000× deformed mesh) (c), crack opening magnitude (d), and crack normal orientations (with every 50th plotted) (e) at the end of simulation.

Figure 3a and 3b show the normalized potential and the magnitude of the electric field in the sample surface at the crest of the first cycle of the excitation, i.e. when the excitation voltage is 50 kV. The excitation causes significant damage in the numerical rock, as attested in Figure 3d and 3e, which results from the major principal stress exceeding 10 MPa at many places. The failure is related to a resonance frequency of the sample, as demonstrated in [6]. The number of cracks, with every 50th normal plotted in Figure 3d, exceeds 100000. However, only some of them open significantly, as can be observed in Figure 3d.

Next, the uniaxial tension test were carried out on intact and piezoelectrically treated samples. In the latter case, the sample after the treatment with the cracks and the softening variable values are set as the initial state for the tension test. However, the cracks were assumed to be closed so that no initial stresses exist in the sample, but only the cracks and their decreased tensile strengths. The results are shown in Figure 4.

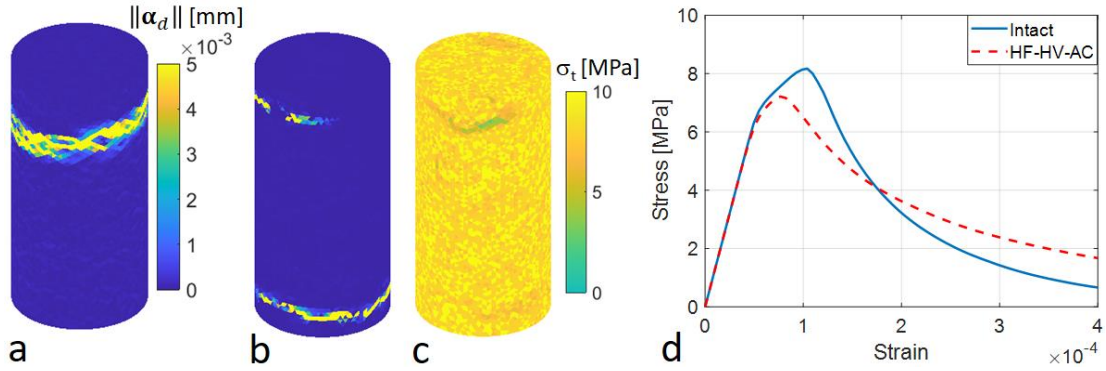

Figure 4. Uniaxial tension test: crack opening magnitude for intact (a) and piezoelectrically treated (b) numerical rock; tensile strength distribution in the piezoelectrically treated sample (c); corresponding stress-strain responses (d).

The resulted failure modes due to pulling the upper surface of the numerical rock at a constant velocity of 5 mm/s attest the experimental transverse splitting of the sample. However, piezoelectrically treated sample (Figure 4b) exhibits the double crack configuration, which is due to the substantially opened initial cracks located at these locations in the piezoelectrically treated sample (see Figure 3d). The tensile strength, as can be read in Figure 4d, is 8.2 MPa for the intact rock and 7.2 MPa for the pre-treated one, which means 12.2 % weakening effect. This is not as large effect as perhaps expected on the basis of the results in Figure 3. This can be explained by the fact that the orientation of the piezoelectrically induced cracks is not optimally favorable for the tension direction, i.e. having the normal parallel to the tension axis (z-axis). It should also be reminded that the tensile strength of a new crack in an element with an initial crack can be close to the strength of the intact mineral if the corresponding crack normals are close to perpendicular.

4. Conclusions

The weakening of the tensile strength of granite by the HV-HF-AC piezoelectric excitation of Quartz was numerically studied. The simulation results suggest that the method has some promise as a potential pre-treatment method in comminution, as the tensile strength of cylindrical numerical granite sample was decreased by 12 % after 500 cycles of sinusoidal excitation at the voltage of 50 kV and frequency of 305 kHz. However, the orientation of cracks, induced by piezoelectric excitation with the positive electrode wrapped around the cylindrical rock sample, is not optimal, i.e. orthogonal, to the tensile loading direction. These finding suggests that more research is needed in order to design the electrode configuration, with respect to the sample shape, so that maximum weakening effect can be obtained. In any case, this work demonstrates the potential of the present method and warrants more research. Most importantly, experimental confirmation of the effect is sorely needed.

Acknowledgements
This research was funded by Academy of Finland under grant number 340192.

References

[1] Klein B, Wang C and Nadolski S 2018 Energy-Efficient Comminution: Best Practices and Future Research Needs. In: Awuah-Offei K, eds. Energy Efficiency in the Minerals Industry. Green Energy and Technology. Springer, Cham, 197–211.
[2] Aditya S, Nandi T K, Pal S K and Majumder AK 2017 Pre-treatment of rocks prior to comminution – A critical review of present practices. *Int J Min Sci. Technol*. **27** 339–348.
[3] Sefiu O A, Hussin A M A and Haitham M A A 2020 Methods of Ore Pretreatment for Comminution Energy Reduction. *Minerals*. **10** 423.
[4] Cho S H, Cheong S S, Yokota M and Kaneko K 2016 The Dynamic Fracture Process in Rocks Under High-Voltage Pulse Fragmentation. *Rock Mech Rock Eng.* **49** 3841–53.
[5] Walsh S D C and Vogler D 2020 Simulating electropulse fracture of granitic rock. *Int J Rock Mech Min Sci.* **128** 104238.
[6] Saksala T 2021 Cracking of granitic rock by high frequency-high voltage-alternating current actuation of piezoelectric properties of quartz mineral: 3D numerical study. *Int J Rock Mech Min Sci.* **147** 104891.
[7] Alexandrov K S and Ryzhova T V 1961 Elastic properties of rock-forming minerals. II. Layered silicates, Izv. Acad. Sci. USSR Geophys. Ser., Engl. Transl. **12** 1165–68.
[8] Brown J M, Angel R J and Ross N L 2016 Elasticity of plagioclase feldspars. *J. Geophys. Res. B: Solid Earth.* **121** 663–675.
[9] Heyliger P, Ledbetter H and Kim S 2003 Elastic constants of natural quartz. *J. Acoust. Soc. Am*. **114** 644–650.
[10] Newnham R E 2005 Properties of Materials: Anisotropy, Symmetry, Structure. Oxford University Press, New York, 2005.